Available online at www.sciencedirect.com
SCIENCE DIRECT®
Journal of Sound and Vibration 285 (2005) 365–390
JOURNAL OF SOUND AND VIBRATION
www.elsevier.com/locate/jsvi

Damage detection of mono-coupled periodic structures based on sensitivity analysis of modal parameters

H.P. Zhu[a,*], Y.L. Xu[b]

[a]*School of Civil Engineering and Mechanics, Huazhong University of Science and Technology, 430074 Wuhan, PR China*
[b]*Department of Civil and Structural Engineering, The Hong Kong Polytechnic University, Kowloon, Hong Kong, China*

Received 6 October 2003; received in revised form 10 March 2004; accepted 26 August 2004
Available online 23 November 2004

Abstract

A sensitivity-based method for localization and assessment of damage in mono-coupled periodic structures is presented in this paper, in which slopes and curvatures of mode shapes are used to localize damage, and natural frequencies are then utilized to quantify the damage. The expressions of sensitivity coefficients of mode shapes, slopes, and curvatures of a mono-coupled periodic system are first derived in terms of receptances of periodic element. A mono-coupled periodic spring-mass system with 10 degrees of freedom is used to carry out a sensitivity study to compare the sensitivities of natural frequencies, mode shapes, slopes, and curvatures to damage. The results show that the sensitivities of these modal parameters in a mono-coupled periodic structure do not depend on the structural parameters, and therefore there is no need for a prior analytical model of the structure. The study also demonstrates that among these modal parameters, curvatures of modal shapes are most sensitive but slopes of mode shapes seem to be more indicative of damage location. A 20-element mono-coupled periodic spring-mass system is adopted to demonstrate the capacity of the proposed method to localize and quantify damages in the mono-coupled periodic system. Finally, a 3-storey near mono-coupled periodic experimental building is used to verify the actual application of the proposed method in consideration of the influence of measurement noise and non-perfect periodicity of actual engineering structures. Numerical and experimental results illustrate that only using a few lower modes with or without noise pollution can accurately detect damages in a mono-coupled periodic or a near mono-coupled periodic structure, either single or multiple damage locations and slight or severe damages.

*Corresponding author. Tel.: +86 27 87556774; fax: +86 27 87545438.
E-mail addresses: hpzhu@mail.hust.edu.cn (H.P. Zhu), ceylxu@polyu.edu.hk (Y.L. Xu).

0022-460X/$ - see front matter © 2004 Elsevier Ltd. All rights reserved.
doi:10.1016/j.jsv.2004.08.012

1. Introduction

In civil engineering structures, it has already been accepted that damage, either local or global, can be observed through changes in dynamic characteristics: natural frequencies, modal damping ratios, mode shapes and their derivatives [1]. This makes vibration-based damage detection techniques attractive in civil engineering applications. Since modal shapes and their derivatives such as slopes and curvatures provide local information of structures, a variety of damage localization methods based on the changes in mode shapes and mode shape derivatives were developed [2]. Shi and Law used incomplete mode shapes to locate the damage of a 31 bar truss structure [3]. Abdo and Hori clarified the relationship between damage characteristics and changes in the rotation of mode shape and found that the rotation of mode shape is promising in detecting and locating damage in structures [4]. Wahab [5], among others [6], demonstrated the use of changes in the curvature mode shape to detect and locate damage in a real bridge and found that the curvature mode shapes are highly sensitive to damage. Wolf and Richardson [7] found that both the modal assurance criterion (MAC) and the coordinate modal assurance criterion (COMAC) were not sensitive enough to detect damage in its earlier stages. Ndambi et al. [8] conducted a comparative study between the use of natural frequencies and mode shape derivatives for damage assessment in reinforced concrete beams. They found that frequencies are affected by accumulation of cracks in the beams and are not influenced by the crack damage locations whereas the MAC and COMAC factors are less sensitive to crack damage compared to frequencies and the strain energy method appears to be more precise than the flexibility matrix method. All these studies showed that using mode shapes and mode shape derivatives could localize damages of structures under some circumstances. However, all methods discussed above require a baseline reference data to obtain the sensitivity coefficients, usually a prior finite element model of the structure in its undamaged condition, which poses a restriction on the applicability in some cases where the analytical model of the undamaged test structures is not available. Parloo et al. [9] presented a mode shape sensitivity-based method for the localization and assessment of damage in which the sensitivity coefficients make no use of the original analytical model. However, the exact sensitivities are calculated on the basis that all mode shapes of the intact structure should be available. In practice, only a limited number of modes can be measured, that is, an approximation of the sensitivities to some content has to be obtained instead.

Engineering structures including multi-storey buildings, elevated guideways for high-speed transportation vehicles (“Maglev” systems), multi-span bridges, chemical pipelines, stiffened plates and shells in aerospace and ship structures, space station structures and layered composite structures, can be considered as a periodic or a near periodic system. Zhu and Wu [10] discussed the sensitivity of natural frequencies to damages in a mono-coupled periodic structure. They found that the sensitivity of natural frequencies does not depend on the structural parameters, and therefore there is no need for the detailed structural parameters of the structures to obtain sensitivity coefficients of natural frequencies. To extend the work [10], the first objective of this paper is to derive the explicit expressions for mode shapes, slopes, and curvatures, consecutively, to obtain the sensitivities of these modal parameters to damages in mono-coupled periodic systems. A mono-coupled periodic spring-mass system with 10 degrees of freedom is then used to discuss and compare the sensitivities of different modal parameters, including natural frequencies, mode shapes, slopes, and curvatures, to damages and their capacity for damage localization. A

two-stage sensitivity-based method, which utilizes slopes and curvatures of mode shapes to localize damage in the first stage and the limited natural frequencies to quantify the damage in the second stage, is proposed to detect damages in a mono-coupled periodic system. A 20-element mono-coupled periodic spring-mass system is adopted to demonstrate the capacity of the proposed method to localize and quantify damages. Finally, a 3-storey mono-coupled near periodic experimental building is used to demonstrate the actual application of the proposed method in consideration of the influence of measurement noise and non-perfect periodicity of actual engineering structures.

2. Sensitivity coefficient analysis

2.1. Sensitivity coefficients

Consider a finite mono-coupled periodic system with one single damage in the jth element and terminating at the general boundaries at extreme end coordinates C and D as shown in Fig. 1. Based on the receptance method, the displacement x_i^d at ith element in terms of the displacement x_0^d at end C is [10]

$$x_i^d = \frac{e^{-i\mu} + \Phi e^{i\mu}}{1+\Phi} x_0^d \quad (i = 1, 2 \ldots, j-1), \tag{1a}$$

$$x_i^d = \frac{(e^{-(N-i)\mu} + \beta e^{(N-i)\mu})[\alpha_{wr}(\alpha_{AA} - \alpha_{wt})e^{-(j-1)\mu} + \alpha_{wt}(\alpha_{AA} - \alpha_{wr})e^{(j-1)\mu}\Phi]}{(1+\Phi)\alpha_{AB}[\alpha_{wr}e^{(N-j)\mu}\beta + \alpha_{wt}e^{-(N-j)\mu}]} x_0^d$$
$$(i = j,\ j+1, \ldots, N) \tag{1b}$$

in which

$$\Phi = -\frac{\begin{array}{c}[\alpha_{AA}\alpha_{BB} - \alpha_{BA}\alpha_{AB} + \alpha_{AA}\alpha_{wt} - \alpha_{BB}\alpha_{wt} - \alpha_{wt}^2]\alpha_{wr}^2\beta e^{(N-2j+1)\mu} \\ +[\alpha_{AA}\alpha_{BB} - \alpha_{AB}\alpha_{BA} + \alpha_{AA}\alpha_{wr} - \alpha_{BB}\alpha_{wt} - \alpha_{wt}\alpha_{wr}]\alpha_{wr}\alpha_{wt}\beta e^{-(N-1)\mu}\end{array}}{\begin{array}{c}[\alpha_{AA}\alpha_{BB} - \alpha_{BA}\alpha_{AB} + \alpha_{AA}\alpha_{wr} - \alpha_{BB}\alpha_{wr} - \alpha_{wr}^2]\alpha_{wt}^2 e^{-(N-2j+1)\mu} \\ +[\alpha_{AA}\alpha_{BB} - \alpha_{AB}\alpha_{BA} + \alpha_{AA}\alpha_{wt} - \alpha_{BB}\alpha_{wr} - \alpha_{wt}\alpha_{wr}]\alpha_{wr}\alpha_{wt}\beta e^{(N-1)\mu}\end{array}}$$

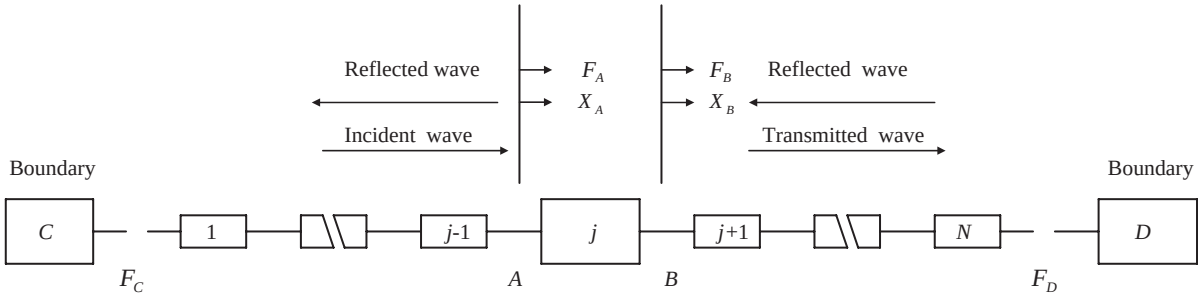

Fig. 1. Block diagram of an N-element periodic system with one damage in the jth element.

$$\beta = -\frac{\alpha_{wr} - \alpha_D}{\alpha_{wt} - \alpha_D}\frac{\alpha_{wt}}{\alpha_{wr}}, \quad \alpha_{wt} = \alpha_{ll} - \alpha_{lr}e^{-\mu}, \quad \alpha_{wr} = \alpha_{ll} - \alpha_{lr}e^{\mu}, \quad \cosh\,\mu = \frac{\alpha_{ll} + \alpha_{rr}}{2\alpha_{lr}},$$

where α_{ll} and α_{rr} are the direct receptances and α_{lr} is the transfer receptance of a periodic element, respectively; α_{AA}, α_{BB} are the direct receptances and α_{AB}, α_{BA} are the transfer receptances of the damaged element, respectively; α_D is the receptance at end D; and μ is the wave propagation constant.

Substituting the nth natural circular frequency, ω_n^d, into Eq. (1) yields the expressions of normalized mode shapes, ϕ_{in}^d, in the nth mode of the damaged periodic structure by specifying $\phi_{Nn}^d = 1$

$$\phi_{in}^d = \frac{(e^{-i\mu} + \Phi e^{i\mu})\alpha_{AB}[\alpha_{wr}e^{(N-j)\mu}\beta + \alpha_{wt}e^{-(N-j)\mu}]}{(1+\beta)[\alpha_{wr}(\alpha_{AA} - \alpha_{wt})e^{-(j-1)\mu} + \alpha_{wt}(\alpha_{AA} - \alpha_{wr})e^{(j-1)\mu}\Phi]} \quad (i = 1, 2, \ldots, j-1; n = 1, 2, \ldots, N), \tag{2a}$$

$$\phi_{in}^d = \frac{e^{-(N-i)\mu} + \beta e^{(N-i)\mu}}{1+\beta} \quad (i = j, j+1, \ldots, N; n = 1, 2, \ldots, N). \tag{2b}$$

For an undamaged periodic structure, the following relations hold on:

$$\alpha_{AA} = \alpha_{ll}, \quad \alpha_{BB} = \alpha_{rr}, \quad \alpha_{AB} = \alpha_{BA} = \alpha_{lr}. \tag{3a–c}$$

Substituting Eq. (3) into Eq. (2) and further simplification then yield the nth normalized mode shapes, ϕ_{in}^u, of the periodic structure without damage by specifying $\phi_{Nn}^u = 1$:

$$\phi_{in}^u = \frac{e^{-(N-i)\mu} + \beta e^{(N-i)\mu}}{1+\beta} \quad (i = 1, 2, \ldots, N; n = 1, 2, \ldots, N). \tag{4}$$

For the periodic structure, the slope of mode shape in the nth mode is defined as

$$\phi'_{in} = \frac{\phi_{in} - \phi_{(i-1)n}}{h} \quad (i = 1, 2, \ldots, N; n = 1, 2, \ldots, N), \tag{5}$$

where ϕ is the mode shape and h is the distance between two successive nodes.

Similarly, the nth mode shape curvature in the nth mode shape is defined as

$$\phi''_{in} = \frac{\phi_{(i+1)n} - 2\phi_{in} + \phi_{(i-1)n}}{h^2} \quad (i = 1, 2 \ldots, N; n = 1, 2, \ldots, N). \tag{6}$$

If an increase of relative flexibility in the jth element, i.e., $\Delta f_j/f$, is used to represent the damage in the jth element, the sensitivities of mode shapes, slopes, and curvatures with respect to damage in the jth element are

$$\bar{S}_{in,j}^{\phi} = \frac{\partial\phi_{in}}{\partial\bar{f}_j} = \lim_{\Delta k_j \to 0}\frac{\phi_{in}^d - \phi_{in}^u}{\Delta f_j/f}; \quad \bar{S}_{in,j}^{\phi'} = \frac{\partial\phi'_{in}}{\partial\bar{f}_j} = \lim_{\Delta k_j \to 0}\frac{\phi_{in}'^{\,d} - \phi_{in}'^{\,u}}{\Delta f_j/f};$$

$$\bar{S}_{in,j}^{\phi''} = \frac{\partial\phi''_{in}}{\partial\bar{f}_j} = \lim_{\Delta f_j \to 0}\frac{\phi_{in}''^{\,d} - \phi_{in}''^{\,u}}{\Delta f_j/f}$$

$$(n = 1, 2, \ldots, N; i = 1, 2, \ldots, N; j = 1, 2, \ldots, N). \tag{7a–c}$$

2.2. Sensitivity coefficient analysis

The N-element mono-coupled periodic spring-mass system with one fixed end C and one free end D (i.e., $\alpha_D = \infty$), which is usually adopted to represent many engineering structures such as multi-storey or highrise buildings in practice, is used here to carry out the sensitivity analysis (see Fig. 2).

The receptances of a periodic element can be expressed as

$$\alpha_{ll} = f - \frac{1}{m\omega^2}, \quad \alpha_{rr} = \alpha_{lr} = \alpha_{rl} = -\frac{1}{m\omega^2}, \tag{8}$$

where m and f are the mass and flexibility of the spring-mass element, respectively, and ω is the vibration circular frequency.

The receptances of the damaged element (i.e., the jth element) are

$$\alpha_{AA} = f + \Delta f_j - \frac{1}{m\omega^2} = \alpha_{ll} + \Delta f_j, \quad \alpha_{AB} = \alpha_{BA} = \alpha_{BB} = -\frac{1}{m\omega^2}, \tag{9}$$

where Δf_j is the change of flexibility in the jth element due to damage.

Substituting Eq. (8) into Eq. (4) yields the nth mode shape of the periodic system without damage

$$\phi_{in}^u = \frac{\cos[(N - i + 0.5)\gamma_n^u]}{\cos \gamma_n^u/2} \quad (i = j, \ldots, N; n = 1, 2, \ldots, N), \tag{10}$$

where $\gamma_n^u = 2\arcsin[\omega_n^u\sqrt{mf}/2]$; and ω_n^u is the nth natural circular frequency of the undamaged periodic system.

Substituting Eqs. (8) and (9) into Eq. (2) yields the nth mode shape of the periodic system with one single damage in the jth element

$$\phi_{in}^d = \frac{\cos(\gamma_n^d/2)\cos[(N - i + 0.5)\gamma_n^d] - 2\alpha_j \sin(\gamma_n^d/2)\sin[(N - j + 1)\gamma_n^d]\cos[(j - i - 0.5)\gamma_n^d]}{\cos^2(\gamma_n^d/2)}$$
$$(i = 1, \ldots, j - 1),$$

$$\phi_{in}^d = \frac{\cos[(N - i + 0.5)\gamma_n^d]}{\cos(\gamma_n^d/2)} \quad (i = j, \ldots, N), \quad (j = 1, 2, \ldots, N; n = 1, 2, \ldots, N), \tag{11a,b}$$

where $\alpha_j = \Delta f_j/f$, and γ_n^d can be obtained by solving Eq. (12)

$$\cos(\gamma_n^d/2)\cos[(N + 0.5)\gamma_n^d] - 2\alpha_j \sin(\gamma_n^d/2)\sin[(N - j + 1)\gamma_n^d]\cos[(j - 0.5)\gamma_n^d] = 0. \tag{12}$$

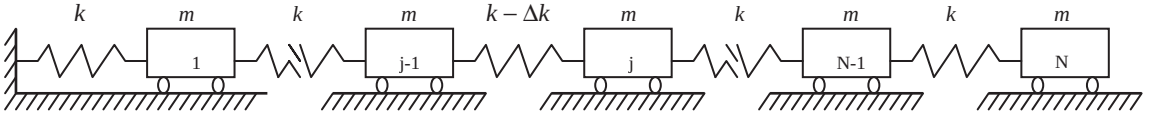

Fig. 2. N-element periodic spring-mass system of one fixed and one free ends with a single damage in the jth element.

Substituting Eqs. (10) and (11) into Eq. (7a) and further simplification yield the sensitivity of nth mode shape

$$S_{in,j}^{\phi} = \frac{\sin(\gamma_n^u/2)\{1+\cos[(2j-1)\gamma_n^u]\}\{0.5\sin[(N-i)\gamma_n^u]+(N-i)\cos(\gamma_n^u/2)\sin[(N-i+0.5)\gamma_n^u]\}}{(N+0.5)\cos^3(\gamma_n^u/2)} - \frac{2\sin(\gamma_n^u/2)\sin[(N-j+1)\gamma_n^u]\cos[(j-i-0.5)\gamma_n^u]}{\cos^2(\gamma_n^u/2)} \quad (i=1,\ldots,j-1),$$

$$S_{in,j}^{\phi} = \frac{\sin(\gamma_n^u/2)\{1+\cos[(2j-1)\gamma_n^u]\}\{0.5\sin[(N-i)\gamma_n^u]+(N-i)\cos(\gamma_n^u/2)\sin[(N-i+0.5)\gamma_n^u]\}}{(N+0.5)\cos^3(\gamma_n^u/2)} \quad (i=j,\ldots,N) \quad (j=1,2,\ldots,N;n=1,2,\ldots,N) \tag{13a, b}$$

The slopes and curvatures of the nth mode shapes of the periodic system without and with one single damage in jth element can be obtained by substituting Eqs. (10) and (11) into Eqs. (5) and (6), respectively. Moreover, the expressions for the sensitivities of slopes and curvatures of the nth mode shape can be derived by using Eqs. (7b) and (7c)

$$S_{in,j}^{\phi'} = -\frac{\sin(\gamma_n^u/2)\{1+\cos[(2j-1)\gamma_n^u]\}\{\sin(\gamma_n^u/2)\cos[(N-i-0.5)\gamma_n^u] + (N-i)\sin(\gamma_n^u)\cos[(N-i)\gamma_n^u]+\cos(\gamma_n^u/2)\sin[(N-i-0.5)\gamma_n^u]\}}{(N+0.5)\cos^3(\gamma_n^u/2)} - \frac{4\sin^2(\gamma_n^u/2)\sin[(N-j+1)\gamma_n^u]\sin[(j-i-1)\gamma_n^u]}{\cos^2(\gamma_n^u/2)} \quad (i=1,\ldots,j-2),$$

$$S_{in,j}^{\phi'} = -\frac{\sin(\gamma_n^u/2)\{1+\cos[(2j-1)\gamma_n^u]\}\{\sin(\gamma_n^u/2)\cos[(N-i-0.5)\gamma_n^u] + (N-i)\sin(\gamma_n^u)\cos[(N-i)\gamma_n^u]+\cos(\gamma_n^u/2)\sin[(N-i-0.5)\gamma_n^u]\}}{(N+0.5)\cos^3(\gamma_n^u/2)} + \frac{2\sin(\gamma_n^u/2)\sin[(N-j+1)\gamma_n^u]\cos[(j-i-0.5)\gamma_n^u]}{\cos^2(\gamma_n^u/2)} \quad (i=j-1),$$

$$S_{in,j}^{\phi'} = -\frac{\sin(\gamma_n^u/2)\{1+\cos[(2j-1)\gamma_n^u]\}\{\sin(\gamma_n^u/2)\cos[(N-i-0.5)\gamma_n^u] + (N-i)\sin(\gamma_n^u)\cos[(N-i)\gamma_n^u]+\cos(\gamma_n^u/2)\sin[(N-i-0.5)\gamma_n^u]\}}{(N+0.5)\cos^3(\gamma_n^u/2)} \quad (i=j,\ldots,N), \quad (j=1,2,\ldots,N;n=1,2,\ldots,N) \tag{14a–c}$$

$$S_{in,j}^{\phi''} = -\frac{2\sin^3(\gamma_n^u/2)\{1+\cos[(2j-1)\gamma_n^u]\}\{\sin[(N-i)\gamma_n^u]+2(N-i)\cos(\gamma_n^u/2)\}}{(N+0.5)\cos^3(\gamma_n^u/2)} + \frac{8\sin^3(\gamma_n^u/2)\sin[(N-j+1)\gamma_n^u]\cos[(j-i-0.5)\gamma_n^u]}{\cos^2(\gamma_n^u/2)} \quad (i=1,\ldots,j-2),$$

$$S_{in,j}^{\phi''} = -\frac{2\sin^3(\gamma_n^u/2)\{1+\cos[(2j-1)\gamma_n^u]\}\{\sin[(N-i)\gamma_n^u]+2(N-i)\cos(\gamma_n^u/2)\}}{(N+0.5)\cos^3(\gamma_n^u/2)} + \frac{4(3-2\cos(\gamma_n^u))\sin(\gamma_n^u/2)\ \sin[(N-j+1)\gamma_n^u]}{\cos(\gamma_n^u/2)} \quad (i=j-1),$$

$$S_{in,j}^{\phi''} = -\frac{2\sin^3(\gamma_n^u/2)\{1+\cos[(2j-1)\gamma_n^u]\}\{\sin[(N-i)\gamma_n^u]+2(N-i)\cos(\gamma_n^u/2)\}}{(N+0.5)\cos^3(\gamma_n^u/2)} - \frac{2\sin(\gamma_n^u/2)\ \sin[(N-j+1)\gamma_n^u]}{\cos(\gamma_n^u/2)} \quad (i=j),$$

$$S_{in,j}^{\phi''} = -\frac{2\sin^3(\gamma_n^u/2)\{1+\cos[(2j-1)\gamma_n^u]\}\{\sin[(N-i)\gamma_n^u]+2(N-i)\cos(\gamma_n^u/2)\}}{(N+0.5)\cos^3(\gamma_n^u/2)} \quad (i=j+1,\ldots,N), \quad (j=1,2,\ldots,N; n=1,2,\ldots,N). \tag{15a–d}$$

From Eqs. (13)–(15) it can be seen that for a periodic spring-mass system, the sensitivities of mode shapes, slopes, and curvatures to damages relate only on the number of the element of the periodic system (N), the mode number (n) and the location of damage (j). They do not depend on structural parameters such as mass and flexibility. Thus, for a periodic spring-mass system, the sensitivities of mode shapes, slopes, and curvatures can be obtained only if the number of the element of the periodic system (N) is known, not requiring physical parameters of the structure.

3. Application of sensitivity analysis

A mono-coupled periodic spring-mass system with 10 elements shown in Fig. 2 is used here to numerically discuss and compare the sensitivities of relative natural frequencies, mode shapes, slopes, and curvatures of the system. The sensitivity of relative natural frequencies with respect to damage is given [10] as

$$\bar{S}_{n,j}^{\omega} = \frac{\partial\bar{\omega}_n}{\partial\bar{f}_j} = \lim_{\Delta f_j\to 0}\frac{(\omega_n^d-\omega_n^u)/\omega_n^u}{\Delta f_j/f}, \tag{16}$$

where ω_n^d is the nth natural circular frequency of the damaged periodic system.

The sensitivity coefficients of relative natural frequencies obtained from Eq. (16) satisfy $\sum_{j=1}^{N}\bar{S}_{n,j}^{\omega} = -0.5$ $(n=1,2\ldots,10)$. The maximum absolute sensitivity coefficients of relative frequencies in the first 10 modes are, respectively, 0.0947 (at $\bar{S}_{1,1}^{\omega}$), 0.0905 (at $\bar{S}_{2,1}^{\omega}$), 0.0920 (at $\bar{S}_{3,9}^{\omega}$), 0.0714 (at $\bar{S}_{4,9}^{\omega}$ and $\bar{S}_{4,10}^{\omega}$), 0.0905 (at $\bar{S}_{5,5}^{\omega}$ and $\bar{S}_{5,10}^{\omega}$), 0.0947 (at $\bar{S}_{6,10}^{\omega}$), 0.0947 (at $\bar{S}_{7,7}^{\omega}$ and $\bar{S}_{7,10}^{\omega}$), 0.0905 (at $\bar{S}_{8,2}^{\omega}$,$\bar{S}_{8,6}^{\omega}$ and $\bar{S}_{8,9}^{\omega}$), 0.0947 (at $\bar{S}_{9,3}^{\omega}$ and $\bar{S}_{9,7}^{\omega}$) and 0.0947 (at $\bar{S}_{10,4}^{\omega}$ and $\bar{S}_{10,6}^{\omega}$). The results indicate that the maximum sensitivity coefficients of relative frequencies change slightly with the mode number.

The sensitivity coefficients of mode shapes are computed based on Eq. (13). The numerical results show that the maximum absolute sensitivity coefficients of the first 10 mode shapes are 0.1336 (at $\bar{S}_{11,1}^{\phi}$), 0.3607 (at $\bar{S}_{12,1}^{\phi}$), 0.5874 (at $\bar{S}_{83,9}^{\phi}$), 0.8571 (at $\bar{S}_{84,9}^{\phi}$, $\bar{S}_{74,10}^{\phi}$ and $\bar{S}_{94,10}^{\phi}$), 1.2927 (at

$\bar{S}^{\phi}_{75,10}$), 1.9419 (at $\bar{S}^{\phi}_{86,10}$), 3.6166 (at $\bar{S}^{\phi}_{87,10}$), 6.0652 (at $\bar{S}^{\phi}_{78,9}$), 12.8716 (at $\bar{S}^{\phi}_{39,7}$) and 34.7385 (at $\bar{S}^{\phi}_{310,4}$), respectively. Compared with the results of natural frequencies, the variation of sensitivity coefficients based on mode shapes is larger and the coefficients increase with the mode number. It is observed from the computed results that for a given mode the mode shape has larger sensitivities with respect to some damaged locations where the natural frequencies are also very sensitive. For example, for the first and second modes, damage in element 1 causes the largest changes in both frequencies and mode shapes; for the third mode, both the frequencies and mode shapes are most sensitive to damage in the ninth element; and for the fourth mode, the most sensitive elements are elements 9 and 10.

Fig. 3 shows the absolute sensitivities of the first three mode shapes with respect to damages in elements 1, 4, 7 and 10, respectively. It is seen that the sensitivities achieve the maximum values at the starting node of the damaged elements. They sharply decrease in the damaged elements and achieve local minimum values at the end of damaged elements, which seems to indicate the locations of damage. The figure also tells us that the maximum absolute sensitivities of mode shapes with respect to a specified damage location do not increase as increasing mode number. For example, the change in the second mode shape due to damage in the 4th element is zero, which is smaller than the change in the first mode shape. The maximum sensitivity of the second mode shape to damage in the 7th element is 0.2711 while the value for the third mode shape is 0.12331.

In order to illustrate the phenomenon observed in Fig. 3, the sensitivity, $S^{\omega}_{n,j}$, of natural frequencies with respective to damage, which represents the change in nth natural frequency for one single damage, is introduced

$$S^{\omega}_{n,j} = \frac{\partial \omega_n}{\partial \bar{f}_j} = \lim_{\Delta f_j \to 0} \frac{\omega^d_n - \omega^u_n}{\Delta f_j / f} = \bar{S}^{\omega}_{n,j} \omega^u_n. \tag{17}$$

The nth natural circular frequency of an undamaged periodic system, ω^u_n, is [10]

$$\omega^u_n = 2\sqrt{\frac{1}{mf}} \sin\left[\frac{\pi}{2}\frac{2n-1}{2N+1}\right]. \tag{18}$$

Obviously, the ratios of different natural frequencies of an undamaged periodic spring-mass system depend only on the number of periodic element (N) and the number of natural frequency (n). For the 10-element mono-coupled periodic spring-mass system, the ratios of the 10 natural frequencies to the first one are 1, 2.978, 4.889, 6.691, 8.343, 9.809, 11.056, 12.056, 12.787 and 13.232, respectively. If the first circular natural frequency of the periodic spring-mass system is assumed to be unity, i.e. $\omega^u_1 = 1$ rad/s, the maximum sensitivity coefficients, $S^{\omega}_{n,j}$, of the 10 natural frequencies are 0.0947, 0.2695, 0.4498, 0.4777, 0.7551, 0.9289, 1.047, 1.0911, 1.2109 and 1.2531, respectively. This indicates that the maximum sensitivity coefficients of natural frequencies increase as the increase in the number of natural frequencies. Fig. 4 shows the absolute sensitivities of the first three natural frequencies with respect to damages in elements 1, 4, 7 and 10, respectively. It is seen from the figure that $S^{\omega}_{2,4} = 0$ and $S^{\omega}_{2,7} = 0.276477 > S^{\omega}_{3,7} = 0.04881$, which matches well with the trends of sensitivities of mode shapes from Fig. 3. The same results for other modes and damages in other elements, which are not given here for clarification, are also observed. This implies that the modes of higher changes in natural frequencies are more sensitive

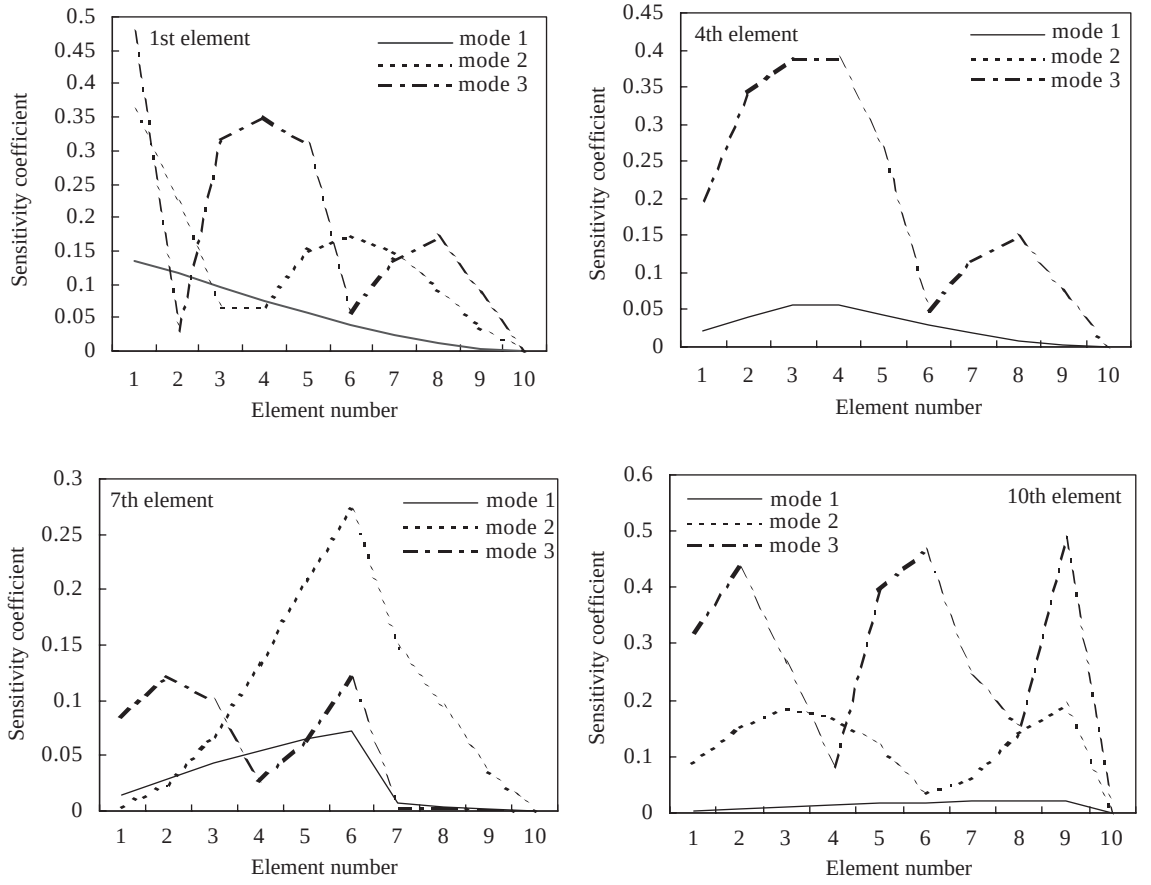

Fig. 3. The absolute sensitivities of the first three mode shapes with respect to damages in elements 1, 4, 7 and 10 of the 10-element periodic spring-mass system.

to damage in mode shapes, and thus it is beneficial for choosing the suitable modes to localize damages.

The sensitivity coefficients of slopes of mode shapes are computed based on Eq. (14). The numerical results show that the maximum absolute sensitivity coefficients of the first 10 modes are 0.1336 (at $\bar{S}^{\phi'}_{11,1}$), 0.4194 (at $\bar{S}^{\phi'}_{72,7}$), 0.7778 (at $\bar{S}^{\phi'}_{43,4}$), 1.2857 (at $\bar{S}^{\phi'}_{34,3}$), 2.1054 (at $\bar{S}^{\phi'}_{95,10}$), 3.6842 (at $\bar{S}^{\phi'}_{96,10}$), 6.0374 (at $\bar{S}^{\phi'}_{37,2}$), 11.6334 (at $\bar{S}^{\phi'}_{78,9}$), 23.8356 (at $\bar{S}^{\phi'}_{39,7}$) and 69.477 (at $\bar{S}^{\phi'}_{410,4}$), respectively. Compared with the results of natural frequencies and mode shapes,the maximum sensitivities of slopes are larger and increase with mode number. The damaged locations that are most sensitive to the slopes are also more sensitive to natural frequencies and mode shapes. Fig. 5 shows the absolute sensitivities of the first three modes with respect to damages in elements 1, 4, 7 and 10, respectively. It can be seen from Fig. 5 that the absolute sensitivity values of the slopes achieve the maximum values at the nodes of the damaged locations, and only one peak occurred in the damaged element for the first mode while there are other peaks for modes 2 and 3 besides the main peak in the damaged element.

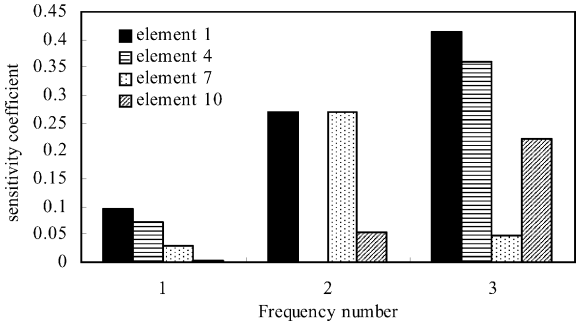

Fig. 4. The absolute sensitivities of the first three natural frequencies with respect to damages in elements 1, 4, 7 and 10 of the 10-element periodic spring-mass system.

Fig. 5 also shows that the maximum sensitivities of the slopes of mode shapes with respect to a specified damage location do not increase as the increase in mode number. For example, the change in the second mode due to damage in the 4th element is zero. The maximum sensitivity of the second mode to damage in 7th element is 0.4194 while the value for the third mode is 0.12186.

The sensitivity coefficients of the curvature mode shapes are computed based on Eq. (15). The numerical results show that the maximum absolute sensitivity coefficients for the first 10 modes are 0.1518 (at $\bar{S}^{\phi''}_{11,1}$), 0.5038 (at $\bar{S}^{\phi''}_{72,8}$), 1.0643 (at $\bar{S}^{\phi''}_{83,9}$), 1.7143 (at $\bar{S}^{\phi''}_{34,3}$ and $\bar{S}^{\phi''}_{84,9}$), 3.3789 (at $\bar{S}^{\phi''}_{95,10}$), 5.4265 (at $\bar{S}^{\phi''}_{96,10}$), 9.7565 (at $\bar{S}^{\phi''}_{87,10}$), 19.6937 (at $\bar{S}^{\phi''}_{78,9}$), 48.0778 (at $\bar{S}^{\phi''}_{39,7}$), and 129.1538 (at $\bar{S}^{\phi''}_{510,9}$),respectively. Compared with the results of natural frequencies, mode shapes, and slopes, the maximum values of the sensitivities of curvature mode shapes are the largest and increase with the mode number. The damaged locations that are the most sensitive to the curvature mode shapes are also more sensitive to natural frequencies, mode shapes and slopes of mode shapes. Fig. 6 shows the absolute sensitivities in the first three modes with respect to damages in elements 1, 4, 7 and 10, respectively. It can be seen from Fig. 6 that the absolute sensitivities of the curvature mode shapes achieve the maximum values between the two nodes of the damaged locations. The observation from Fig. 6 also shows that there is only one peak in the damaged element for the first mode while there are other peaks for modes 2 and 3 besides the main peak in the damaged element. The maximum sensitivities of the curvature mode shapes with respect to a specified damage location do not increase as the increase in mode number. For instance, the change in the second mode due to damage in the 4th element is zero. The maximum sensitivity of the second mode to damage in 7th element is 0.4828 while the value for the third mode is 0.1779.

4. Sensitivity-based damage detection

As mentioned in the above section, the sensitivity coefficients of slopes and curvatures of mode shapes are highly sensitive to damages in a mono-coupled periodic spring-mass system and are indicative of the location of single damage. Since the damaged location which is the most sensitive

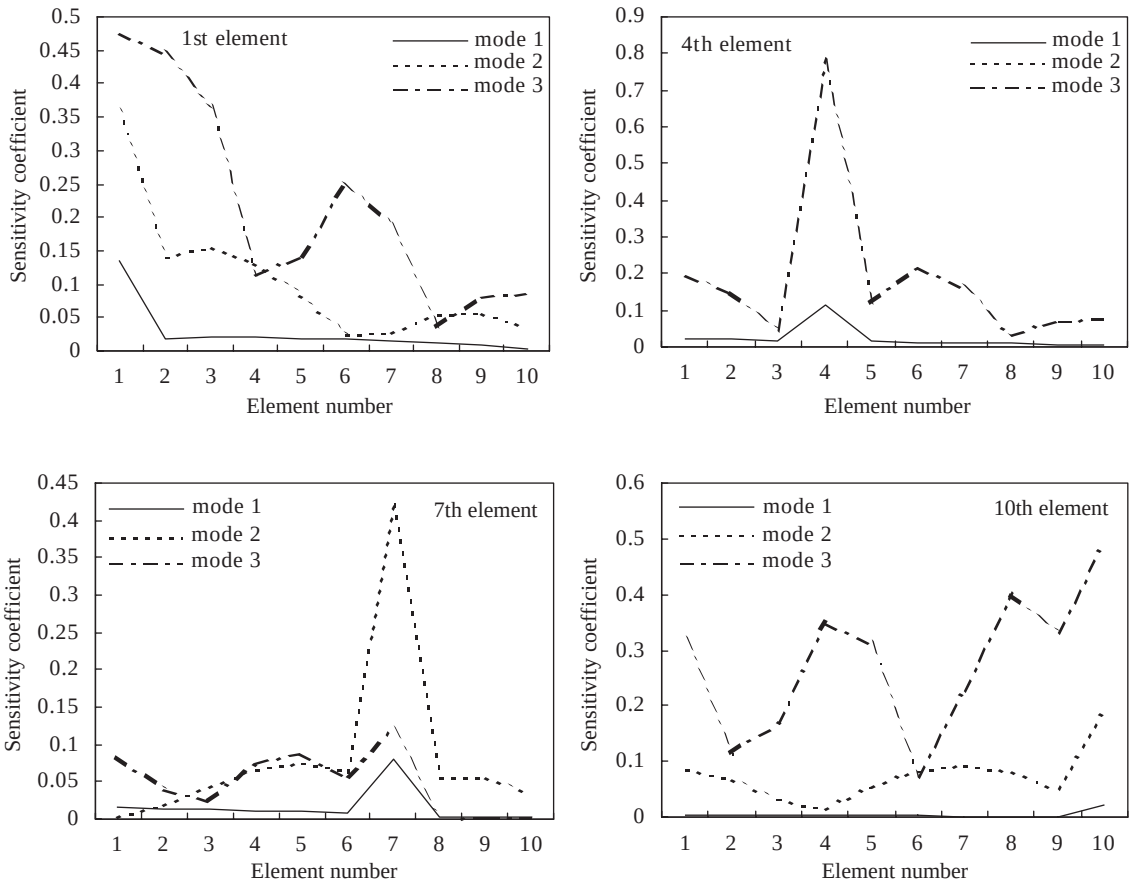

Fig. 5. The absolute sensitivities of slopes of the first three mode shapes with respect to damages in elements 1, 4, 7 and 10 of the 10-element periodic spring-mass system.

to the slope and curvature of a certain mode is also the most sensitive to the corresponding natural frequency for the mono-coupled periodic structure, a few of the mode shapes in which the changes of natural frequencies are larger can be selected to localize multiple damages. The periodic elements with the peaks appearing simultaneously in both the slope and curvature of the mode shape can be considered as potential damage locations. According to this rule, the capacity of the slopes and curvatures of mode shapes to localize single and multiple damages, either slight or severe damage, is explored in this section through numerical and experimental examples. Once the damages are localized, the damage can be quantified from natural frequencies only within the potential damage locations by adopting the first-order approximation from Zhu and Wu [10]

$$\{\Delta\bar{\omega}_n\} = [\bar{S}^{\omega}_{n,j}]\{\alpha_j\}, \tag{19}$$

where $\Delta\bar{\omega}_n = (\omega_n^d - \omega_n^u)/\omega_n^u$ is the relative change of the nth circular natural frequency.

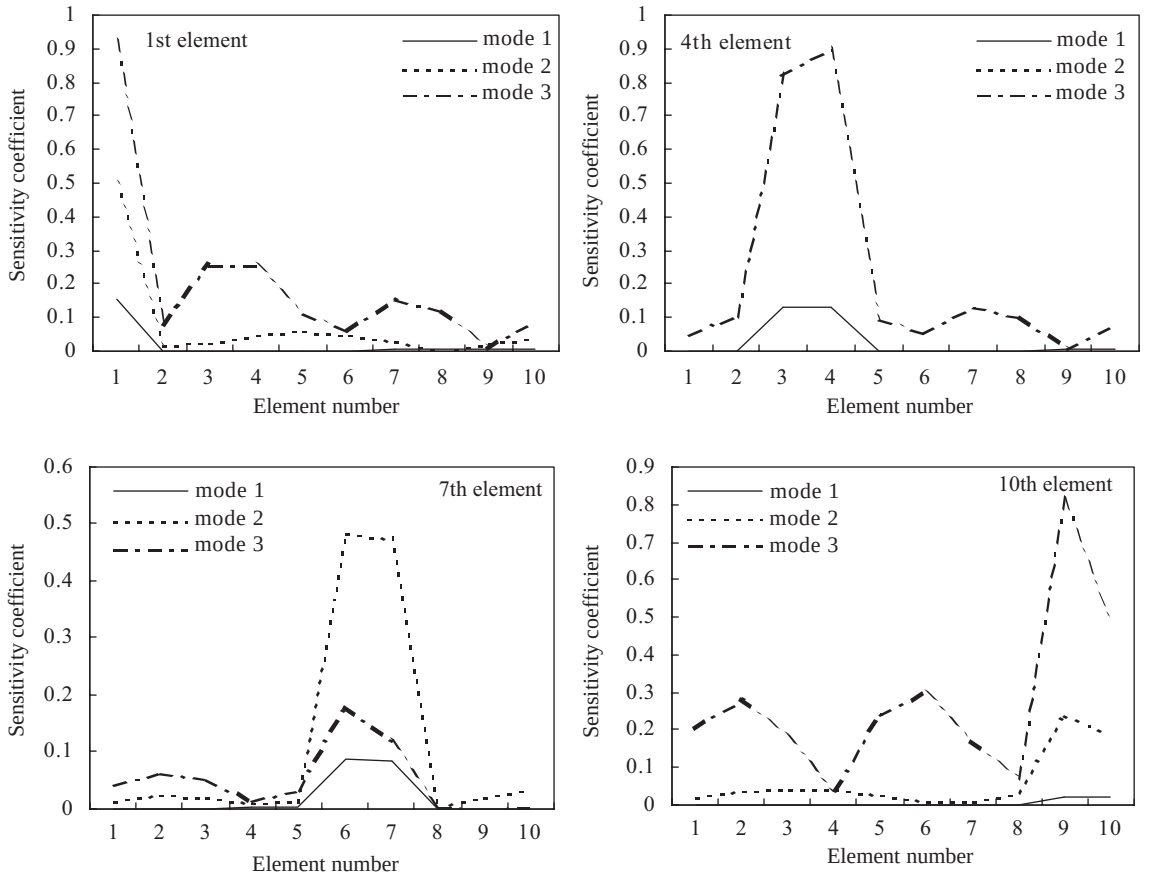

Fig. 6. The absolute sensitivities of curvatures of the first three mode shapes with respect to damages in elements 1, 4, 7 and 10 of the 10-element periodic spring-mass system.

In this study, an optimization solution can be found by minimizing the following matrix norm g under the inequality constraint:

$$g = \|[\bar{S}_{n,j}]\{\alpha_j\} - \{\Delta\bar{\omega}_n\}\| \quad \{\alpha_j \geqslant 0\}. \tag{20}$$

4.1. Numerical example

To assess the performance of the proposed method, the 20-element mono-coupled periodic spring-mass system used in [10] is adopted. Eleven cases representing slight damage (5% flexibility increase), middle damage (10% and 20% flexibility increase) and severe damage (30% flexibility increase) in one or multiple elements, and the changes in the first three natural frequencies are listed in Table 1.

4.1.1. Damage localization

The slope and curvature of mode shape in one of the first three modes, in which the change of natural frequency is the largest (underlined in Table 1), are used to localize damages of the 20-element periodic spring-mass system for each damage scenario. Fig. 7 shows the absolute changes of the slope and curvature of the 3rd mode shape before and after damage in damage scenarios 1, 2 and 3, which represent a slight damage that occurred in single element, respectively. It is seen that the peaks appear simultaneously in both the slope and curvature of the 3rd mode shape at elements 1, 10, and 20 in scenarios 1, 2 and 3, respectively. Fig. 8 shows the absolute changes of the slope and curvature of the 3rd mode shape in damage scenario 7 where there are multiple slight damages with the same damage size. It is seen again that the peaks appear simultaneously in both the slope and curvature of the 3rd mode shape at elements 1, 10 and 20. Fig. 9 shows the results for damage scenarios 9, 10 and 11, which represent the multiple damages with different damage sizes, respectively. For scenario 9, the peaks appear simultaneously in both the slope and curvature of the 3rd mode shape at elements 1, 10 and 20. For scenario 10, the peaks appear simultaneously in both the slope and curvature of the 3rd mode shape at elements 1, 4, 10 and 20. The same observation can be made for scenario 11. The results for damage scenarios 4, 5 and 6, representing single severe damage, have the same trends as those for damage scenarios 1, 2 and 3, which are not given here for clarification. The results for damage scenario 8, where multiple severe damages with the same size exist, are the same as those for damage scenario 7. It can be seen from these figures that the damages in single or multiple locations, either slight or severe damage, can be accurately localized by the slope or curvature of mode shape in only the third mode in which the change of natural frequency is the largest within the first 3 modes. The figures also indicate that the absolute changes of mode shape curvatures at the damaged locations are larger than those of the slopes of mode shapes, but the results for the slopes of mode shapes seem more indicative of damage locations.

4.1.2. Damage quantification

The relative changes of the first three natural frequencies in the 11 damage scenarios listed in Table 1 are used to detect the sizes of the damages within the damage locations identified by the slope and curvature of mode shapes. To illustrate the influence of the number of available natural frequencies on damage detection, the first, the first two and the first three natural frequencies are used, respectively.

Fig. 10 shows the damage quantification results for single and slight damage cases (scenarios 1–3). Fig. 11 shows the results of detection of single severe damage (scenarios 4–6) and Fig. 12 shows the detection of multiple damages with the same size (scenarios 7 and 8). The results in Figs. 10–12 tell us that the sizes of damages in these scenarios can be accurately identified, and the degree of accuracy of detection is not affected by the number of the natural frequencies used. Using only one of the lower natural frequencies, even the first natural frequency, is capable of accurately quantifying the damage in one single location, or damages of the same size in multiple locations, either slight or severe damages.

Fig. 13 shows the detection of multiple damages with different damage sizes (scenarios 9–11). The results demonstrate that the degree of accuracy of damage size detection depends on the number of available measured frequencies. For example, only the first frequency is not sufficient to quantify correctly the damages in these scenarios. As the number of potential damaged

Table 1
Damage scenarios and the corresponding frequency changes for the 20-element periodic spring-mass system

Mode no.	Frequency change $\Delta\omega_i$ and $\Delta\omega_i/\omega_i$ in percentage due to damage											
	Scenario 1		Scenario 2		Scenario 3		Scenario 4		Scenario 5		Scenario 6	
	Element	Damage (%)	Element	Damage (%)	Element	Damage (%)	Element	Damage (%)	Element	Damage (%)	Element	Damage (%)
	1	5	10	5	20	5	1	30	10	30	20	30
1	−0.008 (−0.245%)		−0.004 (−0.137%)		−0.0 (−0.0%)		−0.045 (−1.434%)		−0.025 (−0.804%)		−0.00 (−0.01%)	
2	−0.023 (−0.240%)		−0.008 (−0.081%)		−0.001 (−0.013%)		−0.133 (−1.412%)		−0.046 (−0.484%)		−0.007 (−0.078%)	
3	−0.037 (−0.234%)		−0.029 (−0.188%)		−0.005 (−0.035%)		−0.212 (−1.358%)		−0.174 (−1.112%)		−0.033 (−0.212%)	
	Scenario 7		Scenario 8		Scenario 9		Scenario 10		Scenario 11			
	Element	Damage (%)	Element	Damage (%)	Element	Damage (%)	Element	Damage (%)	Element	Damage (%)	Element	Damage (%)
	1	5	1	30	1	30	1	30	1	30	15	10
	10	5	10	30	10	10	4	10	4	10	20	30
	20	5	20	30	20	10	10	5	10	20		
							20	20				
1	−0.012 (−0.379%)		−0.079 (−2.215%)		−0.053 (−1.700%)		−0.063 (−2.005%)		−0.078 (−2.477%)			
2	−0.031 (−0.334%)		−0.188 (−1.999%)		−0.151 (−1.609%)		−0.164 (−1.747%)		−0.232 (−2.470%)			
3	−0.071 (−0.453%)		−0.402 (−2.573%)		−0.273 (−1.765%)		−0.261 (−1.671%)		−0.395 (−2.531%)			

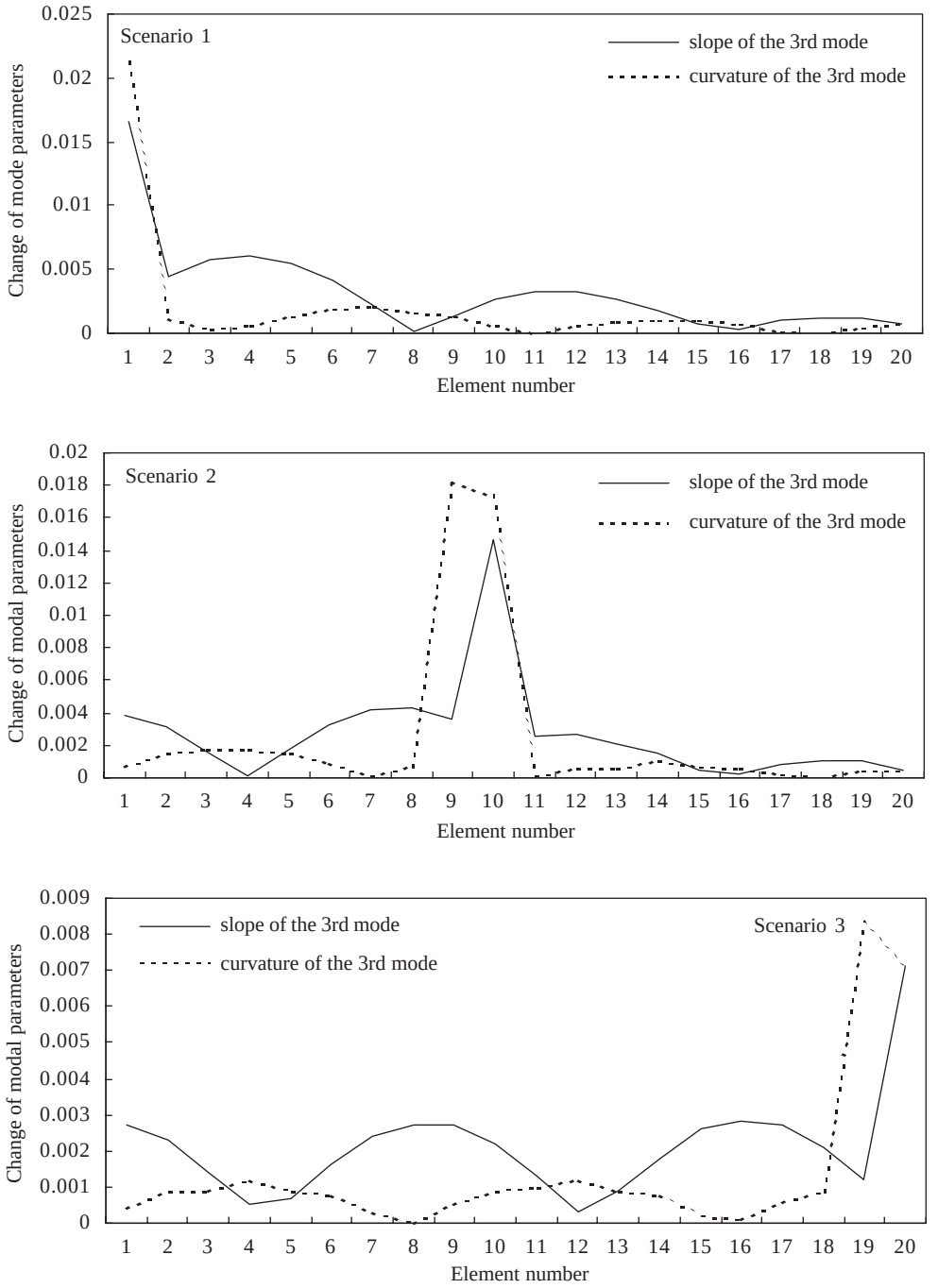

Fig. 7. The absolute changes of slope and curvature of the third mode shape due to damages in the 20-element periodic spring-mass system in scenarios 1, 2 and 3.

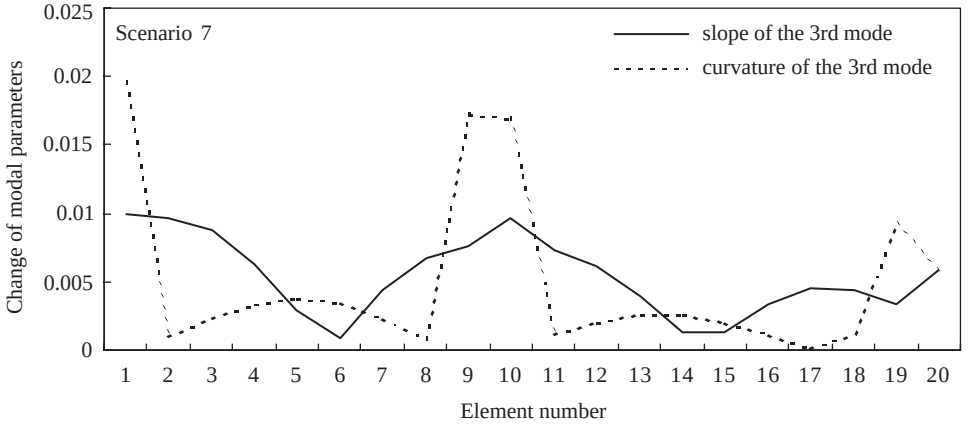

Fig. 8. The absolute changes of slope and curvature of the third mode shape due to damages in the 20-element periodic spring-mass system in scenario 7.

locations increases, an appropriate amount of available natural frequencies is necessary to accurately identify the sizes of multiple damages. It is seen that for scenario 9, in which damages occur in three locations, the damage in element 20 is identified with a large error. For scenarios 10 and 11, where there are damages in 4 and 5 locations, the damage in element 20 cannot be identified if only the first natural frequency is used. If all the damages in 4 or 5 locations in scenarios 10 or 11 are accurately identified, respectively, the 3 natural frequencies should be used. Compared with the results in [10], the degree of accuracy for damage detection is improved largely and the number of used frequencies decreases due to the accurate localization of damages in the first step.

4.2. Experimental verification

The numerical example of the 20-element spring-mass system given in the above section is a perfect mono-coupled periodic structure, and the modal parameters are measurement noise free. To consider the influence of some actual factors such as measurement noise and non-perfect periodicity of structures on the application of the proposed method, a 3-storey mono-coupled near periodic experimental building is used.

4.2.1. Description of experimental model and damage scenarios

The building model was constructed using 3 steel plates of $850 \times 500 \times 25\,\text{mm}^3$ and 4 equally sized rectangular columns of $9.5 \times 75\,\text{mm}^2$ (shown in Fig. 14). The plates and columns were properly welded to form rigid connections. The building was then welded on a steel base plate of 20 mm thickness. The steel base plate was in turn bolted firmly on a shaking table using a total of 8 bolts of high tensile strength. The overall dimensions of the building were $1450 \times 850 \times 500\,\text{mm}^3$. All the columns were made of high strength steel of 435 MPa yield stress and 200 GPa modulus of elasticity. The $9.5 \times 75\,\text{mm}^2$ cross-section of the column was arranged in such a way that the first natural frequency of the building was much lower in the x-direction than in the

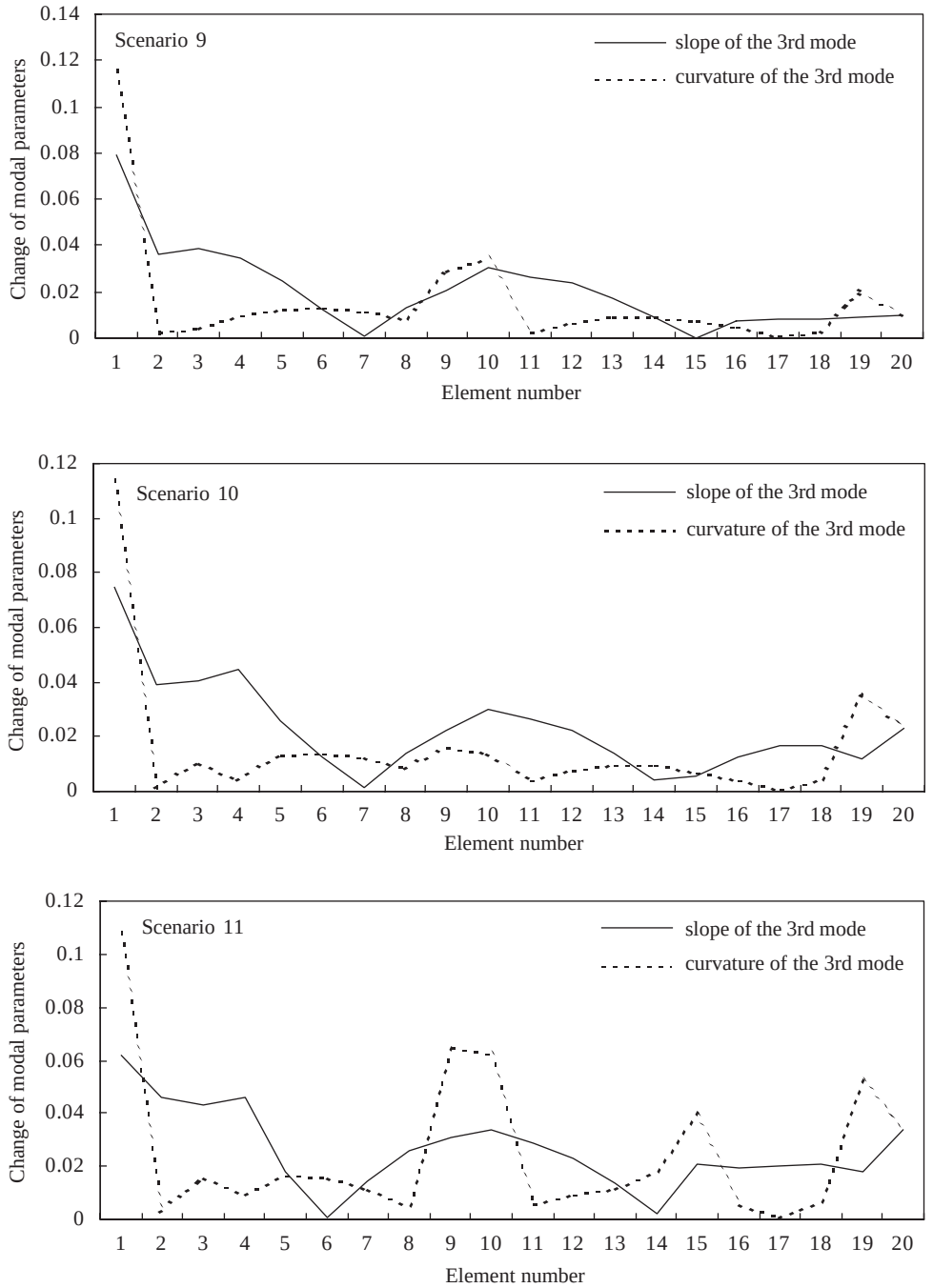

Fig. 9. The absolute changes of slope and curvature of the third mode shape due to damages in the 20-element periodic spring-mass system in scenarios 9–11.

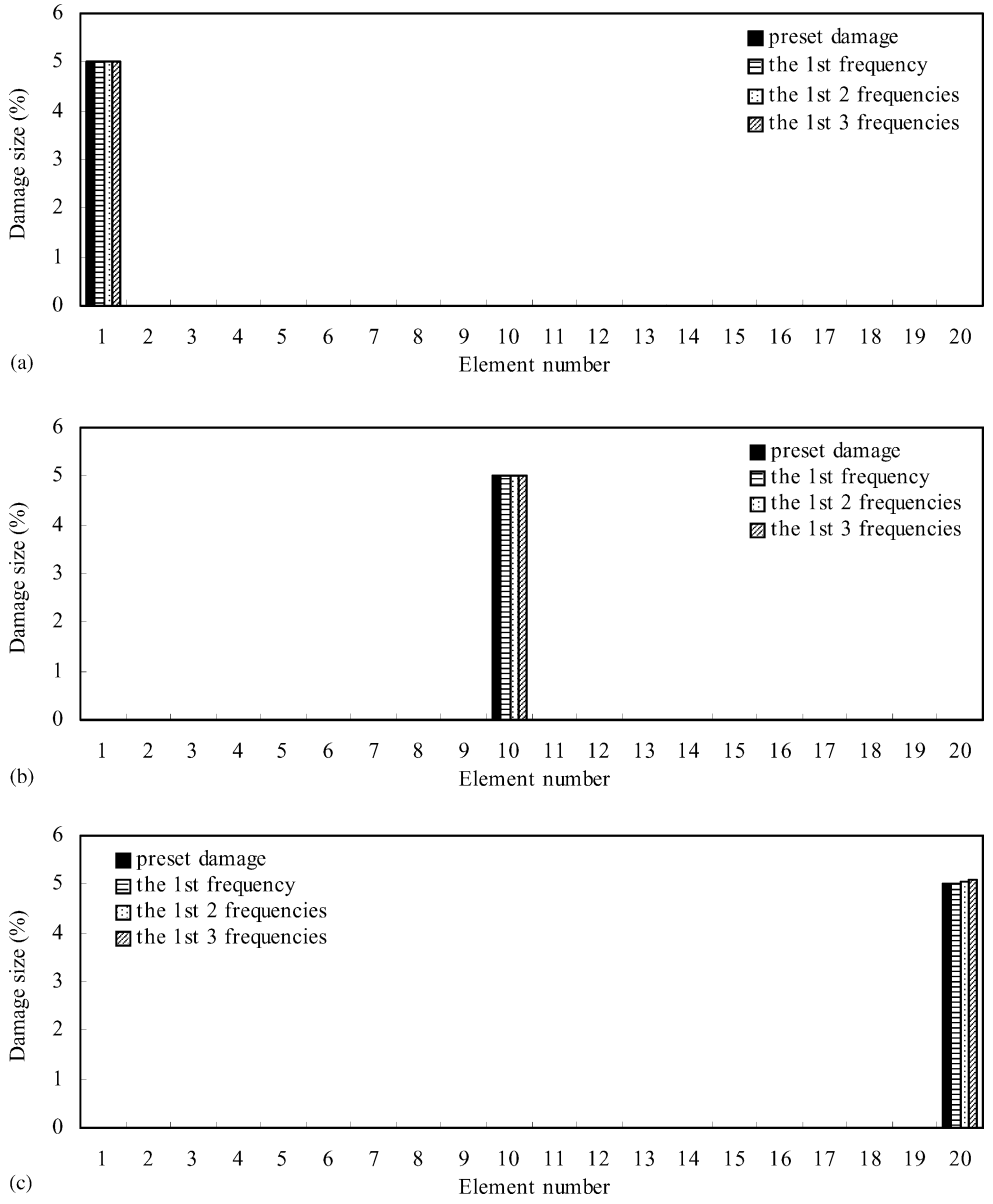

Fig. 10. Detection of single light damage in the 20-element periodic spring-mass system: (a) scenario 1, (b) scenario 2, (c) scenario 3.

y-direction. This arrangement restricted the building motion in the x-direction and thus the building was effectively reduced to planar building in the x–z plane. The thickness of each steel floor was 25 mm so that the floor can be regarded as a rigid plate in the horizontal direction, leading to a shearing type of deformation. The geometric scale of the building model was assumed to be $\frac{1}{5}$. To have a proper simulation, an additional mass block of 135 kg was placed on each floor of the building model.

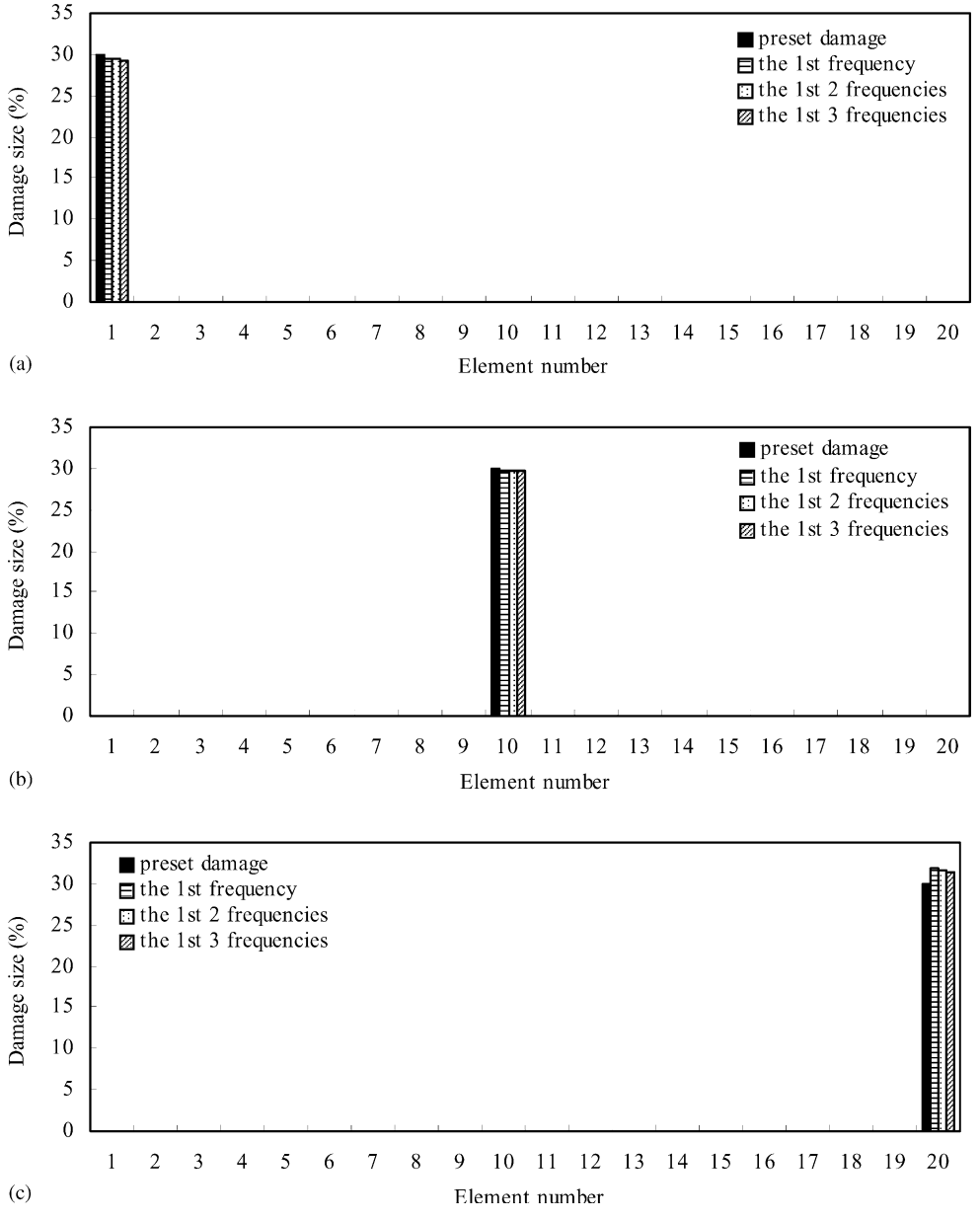

Fig. 11. Detection of single severe damage in the 20-element periodic spring-mass system: (a) scenario 4, (b) scenario 5, (c) scenario 6.

The building model was subjected to a white noise random ground excitation generated by a $3 \times 3\,m^2$ MTS shaking table of The Hong Kong Polytechnic University. Each building floor was equipped with one B&K 4370 accelerometer in the x-direction. The signals from the accelerometers were analysed by commercial computer software ARTeMIS, developed by

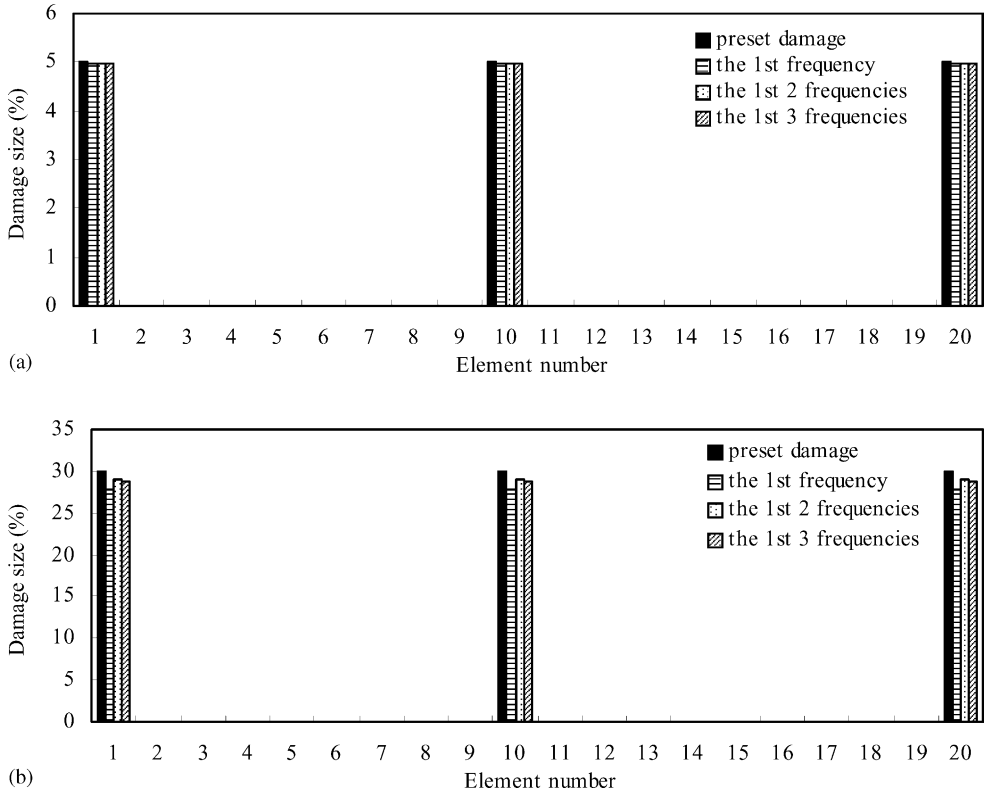

Fig. 12. Detection of multiple damages with the same size in the 20-element periodic spring-mass system: (a) scenario 7, (b) scenario 8.

Structural Vibration Solutions in Denmark, to identify the natural frequencies and mode shapes using the method of Frequency Domain Decomposition (FDD).

Four damage scenarios are considered in the experimental studies. Table 2 lists the four damage scenarios and the corresponding changes in the three natural frequencies. It is noted that in the cases of multiple damages, the damages occur in the two successive elements. The four damage scenarios were implemented step by step by cutting the width of the columns in the first storey to 51.30 mm (scenario 1) and then to 37.46 mm (scenario 2) within a height of 60 mm from the bottom, followed by cutting the width of the columns in the second storey to 51.30 mm (scenario 3) and then to 37.46 mm (scenario 4) within a height of 60 mm from the second floor.

4.2.2. Damage localization

The test building has only 3 degrees of freedom and it is impossible for two peaks to appear in two successive freedoms of a curve. Thus, two modes in which the changes of natural frequencies are larger are chosen (underlined in Table 2). Fig. 15 plots the slopes and curvatures of mode shapes in two of the three modes for damage scenarios 1 and 3, respectively. The slopes and curvatures of mode shapes in damage scenarios 2 and 4 are not given here because their trends are

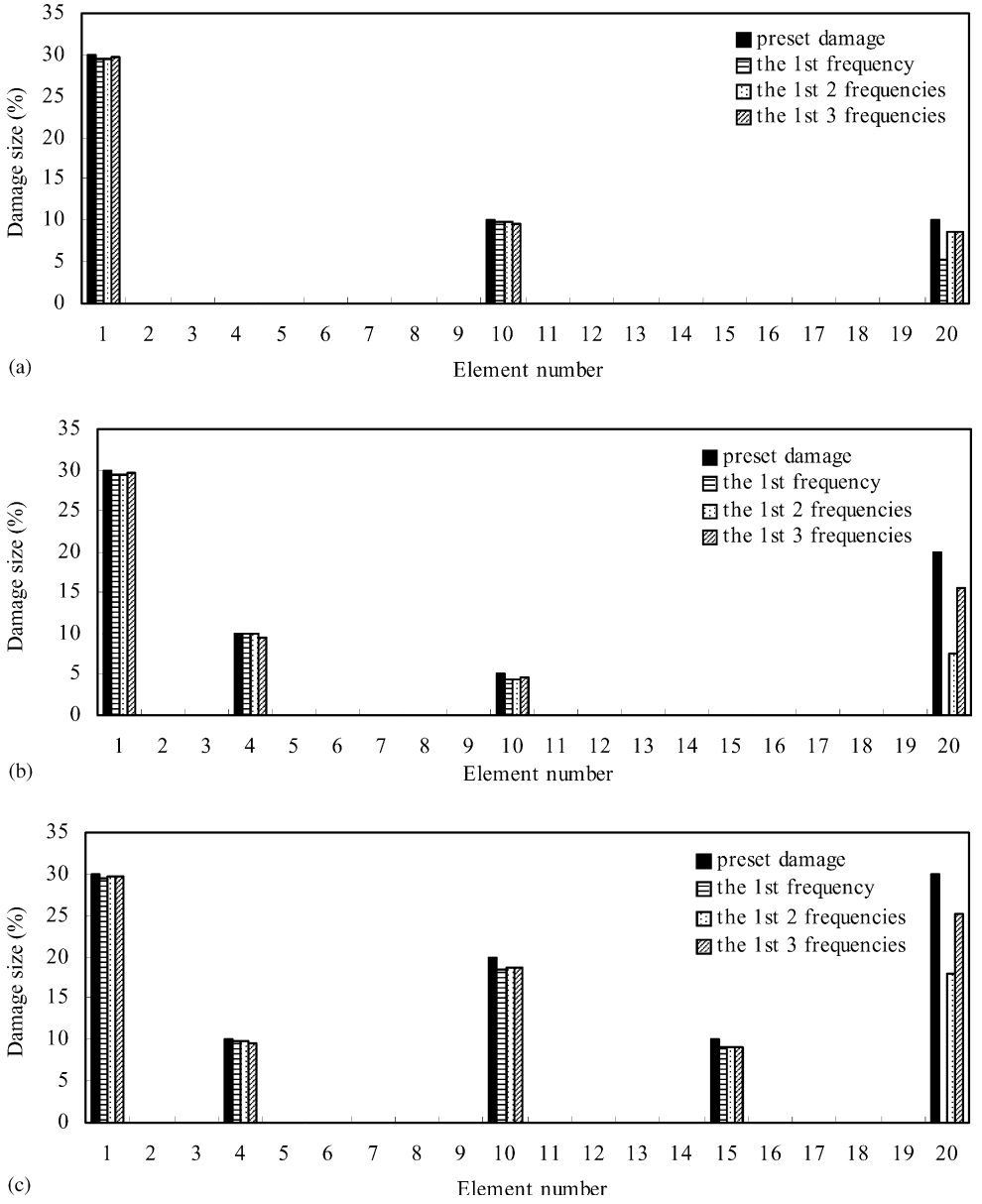

Fig. 13. Detection of multiple damages with different sizes in the 20-element periodic spring-mass system: (a) scenario 9, (b) scenario 10, (c) scenario 11.

in agreement with those in scenarios 1 and 3, respectively. The results from Fig. 15 show that for scenario 1, element 1 is correctly considered as the possible damaged location by the slopes and curvatures of the first and second mode shapes. For damage scenario 3, element 1 is correctly identified as a possible damage location by the slope and curvature of the first mode shape and by

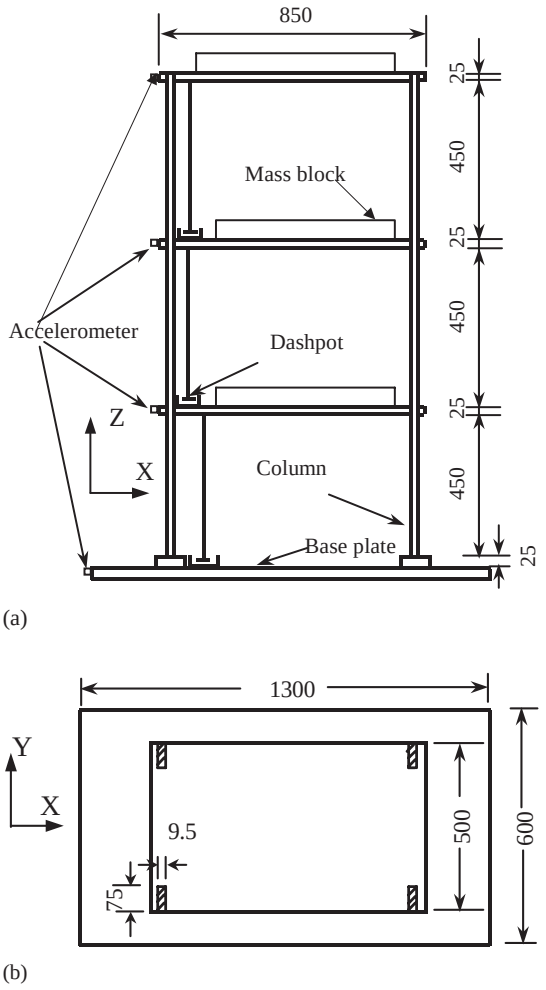

Fig. 14. Configuration of a 3-storey near periodic building: (a) elevation, (b) plan (all dimensions in mm).

the curvature of the second mode shape. Element 2 can be correctly localized by the slope of the first mode shape and by the slope and curvature of the second mode shape.

4.2.3. Damage quantification

To compare the effectiveness of incomplete measured natural frequencies on damage detection, the relative changes in the first, the first two and all the three measured natural frequencies are used to identify the damage, respectively. Fig. 16 shows the results of damage detection for different damage scenarios by using the three groups of measured frequencies. In scenario 1, the damage occurring in the first storey is identified as 12.00%, 12.44% and 12.46% by using the first one, the first two and the three natural frequencies, respectively, which slightly deviate from the preset damage of 13.12%. In scenario 2, the first storey of 27.99%, 25.84% and 25.55% damage

Table 2
Damage scenarios and the corresponding frequency changes for the 3-storey near periodic test building

Mode no.	Frequency change $\Delta\omega_i$ and $\Delta\omega_i/\omega_i$ in percentage due to damage											
	Scenario 1		Scenario 2		Scenario 3				Scenario 4			
	Storey	Damage	Storey	Damage	Storey	Damage	Storey	Damage	Storey	Damage	Storey	Damage
	1	13.12%	1	26.74%	1	26.74	2	13.12	1	26.74	2	26.74
1	−0.6897 (−3.26%)		−1.6080 (−7.60%)		−1.8407 (−8.70%)				−2.2977 (−10.86%)			
2	−1.3712 (−2.25%)		−2.5230 (−4.14%)		−3.2116 (−5.27%)				−3.9063 (−6.41%)			
3	−0.4574 (−0.51%)		−0.9149 (−1.02%)		−3.9016 (−4.35%)				−5.9734 (−6.66%)			

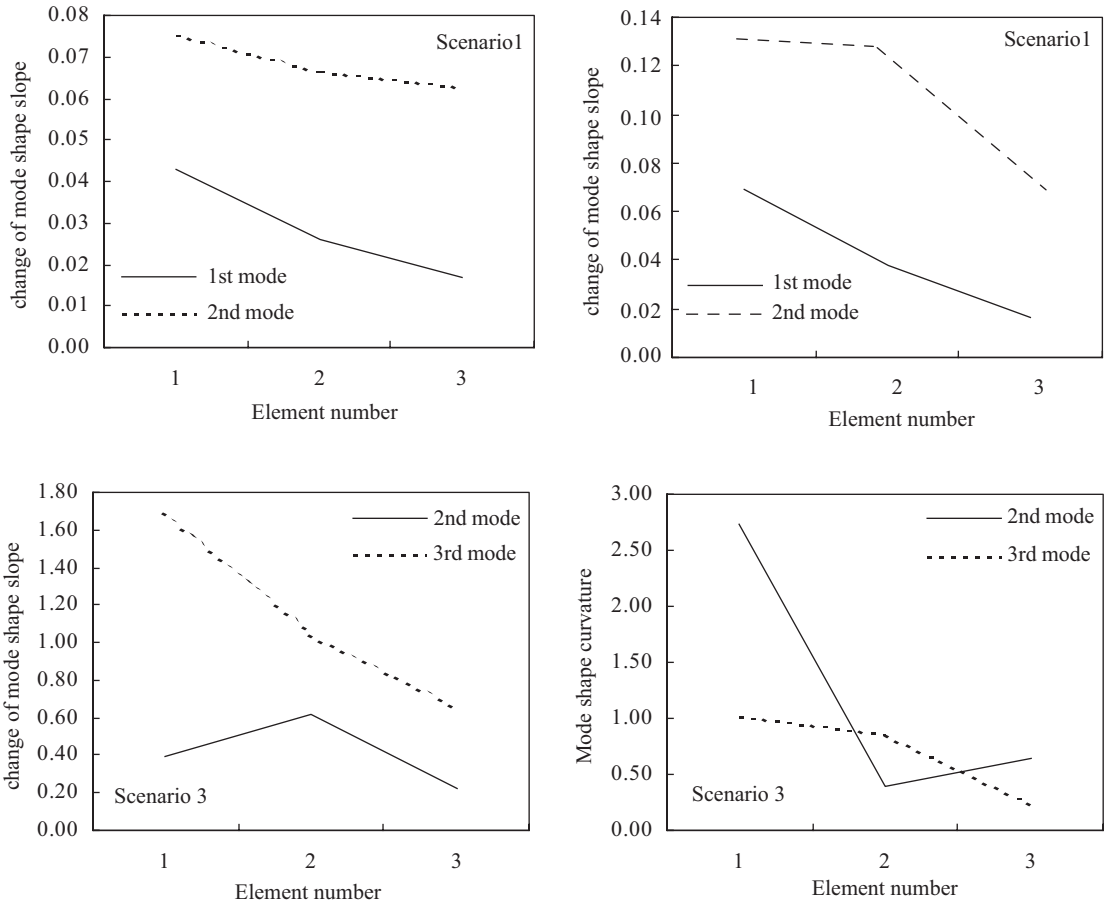

Fig. 15. The absolute changes of slopes and curvatures of mode shapes due to damages in the 3-storey near periodic test building in scenarios 1 and 3.

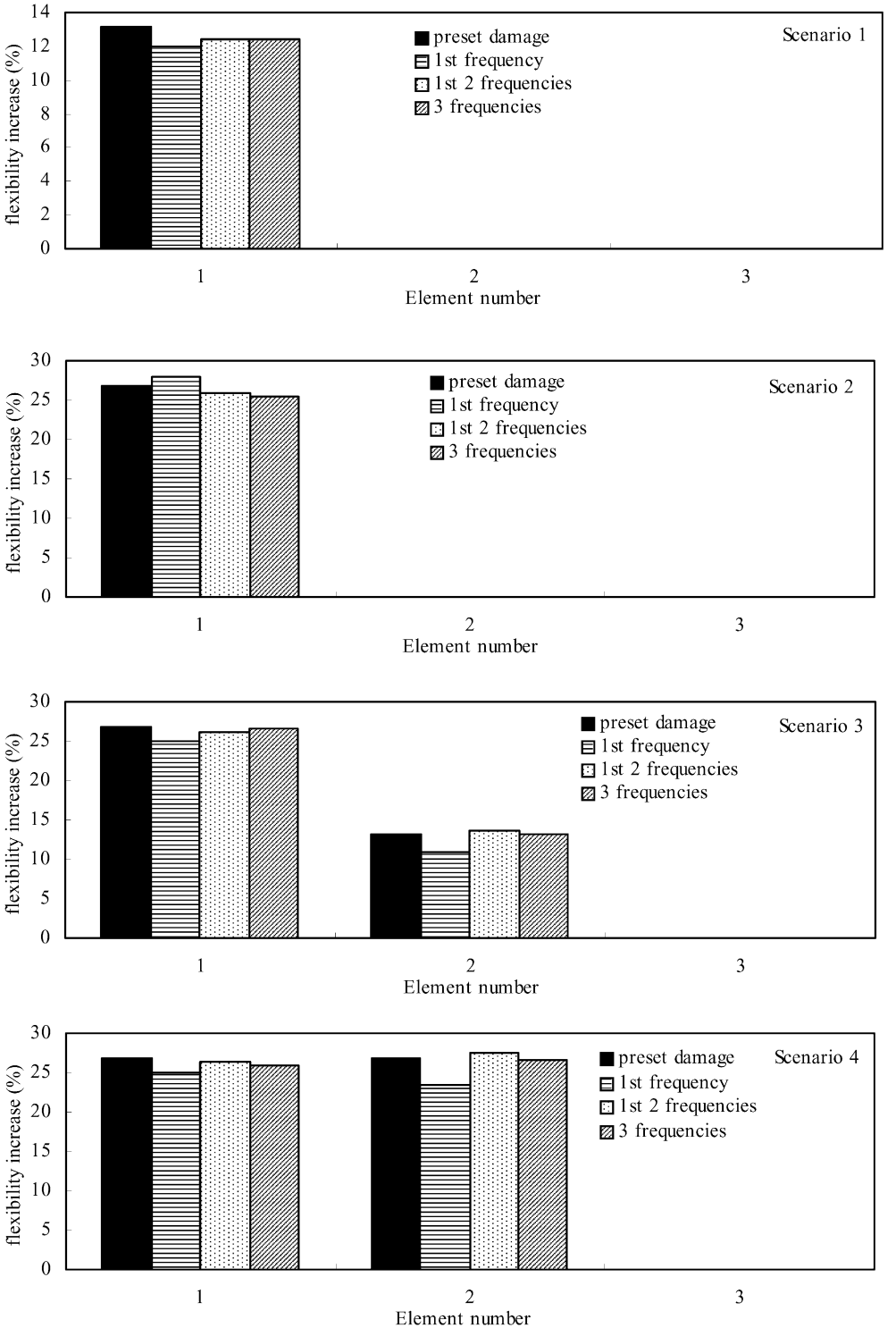

Fig. 16. Detection of damages in the 3-storey near periodic test building in the 4 scenarios.

size is identified using the first one, the first two and the three natural frequencies, respectively, as compared with the preset damage of 26.74%. It is seen that the accuracy of predicting damage size in scenario 2 (severe single damage) does not increase as the increase in the number of used frequencies. This result may be attributed to many factors including the possible measurement errors in the second and third natural frequencies. Nevertheless, the damage size predicted using the three natural frequencies is very close to that using the first two natural frequencies. The identified damage sizes of the first storey are about 25.0%, 26.2% and 26.6%, and about 10.94%, 13.60% and 13.10% for the second storey by using the first one, the first two and the three frequencies in scenario 3, respectively. The identified damages of the first storey are about 25.0%, 26.3% and 25.8%, and about 23.31.94%, 27.60% and 26.5% for the second storey by using the first one, the first two, and the three frequencies in scenario 4, respectively. The identified damages sizes in the multiple damages cases by the two or three natural frequencies match better with the preset ones than those by the first frequency only. However, even if only the first frequency is used, the differences between the predicted and preset ones are not significant. The satisfactory identified results clearly demonstrate that the proposed approach is still suitable and workable for damage detection of actual near mono-coupled periodic structures and robust for the measurement noise.

5. Conclusions

In this paper, the sensitivity coefficients of mode shapes, slopes and curvatures of mode shapes of a mono-coupled periodic structure with respect to damage have been derived. For a mono-coupled periodic spring-mass system, these sensitivity coefficients do not depend on structural parameters, such as stiffness and mass, and thus avoid the requirement of an analytical model of the system in damage detection. The comparative study of a 10-element mono-coupled periodic spring-mass system shows that among natural frequencies, mode shapes, slopes and curvatures, the mode shape curvatures are the most sensitive to damage, but the slopes of mode shapes are more indicative of damage location. The larger changes in the natural frequencies imply higher sensitivity of these modes to damage, which is beneficial for choosing a few of the lower modes to localize the damage.

A two-stage sensitivity-based method, which utilizes the slopes and curvatures of mode shapes to localize damages and limited natural frequencies to quantify damages of mono-coupled periodic systems, has been presented. Numerical results of a 20-element mono-coupled periodic spring-mass system show that single and multiple damages, either slight or severe damages, can be accurately localized using a few of the slope and curvature of the lower mode shapes. For single or multiple damages with the same size, the size of the damage can be identified accurately using only the first frequency, and for multiple damages with different sizes, the accuracy for identifying the damage size depends on the number of used frequencies. The 3-storey near mono-coupled periodic building model has also been investigated experimentally to further consider the influence of some actual factors such as measurement noise and non-perfect periodicity of structures on the application of the proposed method. The experimental results show that the proposed method can accurately detect either slight or severe damages in single and multiple locations in near mono-coupled periodic structures and it is robust for measurement of noise pollution.

Acknowledgements

The authors are grateful for the financial support from The Hong Kong Polytechnic University through its Area of Strategic Development Program in System Identification, Health Monitoring and Damage Detection. The joint support from the National Natural Science Foundation of China (No. 50378041) and the Specialized Research Fund for the Doctoral Program of Higher Education (No. 20030487016) to the first author is also greatly appreciated.

References

[1] B.D. Zakic, Vibrations in diagnosis of damages in concrete bridges, in: *Proceedings of the Second RILEM International Conference on Diagnosis of Concrete Structures*, Strbske Pleso, Slovakia, 1996, pp. 320–326.
[2] J.T. Kim, Y.S. Ryu, H.M. Cho, N. Stubbs, Damage identification in beam-type structures: frequency-based method vs mode-shape-based method, *Engineering Structures* 25 (2003) 57–67.
[3] Z.Y. Shi, S.S. Law, L.M. Zhang, Damage detection by directly using incomplete mode shapes, *Journal of Engineering Mechanics* 126 (6) (2000) 656–660.
[4] M.A.-B. Abdo, M. Hori, A numerical study of structural damage detection using changes in the rotation of mode shapes, *Journal of Sound and Vibration* 251 (2) (2002) 227–239.
[5] M.M.A. Wahab, Damage detection in bridges using modal curvatures: application to a real damage scenario, *Journal of Sound and Vibration* 226 (2) (1999) 217–235.
[6] A.K. Pandey, M. Biswas, M.M. Samman, Damage detection from changes in curvature mode shapes, *Journal of Sound and Vibration* 145 (2) (1991) 321–332.
[7] T. Wolf, M. Richardson, Fault detection in structures from changes in their modal parameters, in: *Proceedings of the Seventh International Modal Analysis Conference*, Las Vegas, Nevada, USA, vol.1, 1989, pp. 87–94.
[8] J.-M. Ndambi, J. Vantomme, K. Harri, Damage assessment in reinforced concrete beams using eigenfrequencies and mode shape derivatives, *Engineering Structures* 24 (2002) 510–515.
[9] E. Parloo, P. Guillaume, M. Van Overmeire, Damage assessment using mode shape sensitivities, *Mechanical Systems and Signal Processing* 17 (3) (2003) 499–518.
[10] H. Zhu, M. Wu, The characteristic receptance method for damage detection in large mono-coupled periodic structures, *Journal of Sound and Vibration* 251 (2) (2002) 241–259.